JOC The Journal of Organic Chemistry

pubs.acs.org/joc Article

Molecular Dynamics of the Davies Ambimodal C−H Functionalization/Cope Rearrangement Reaction

Yaling Zhang, Chaoqin Cao, Yuanbin She, Huw M. L. Davies,* Yun-Fang Yang,* and K. N. Houk*

Cite This: J. Org. Chem. 2024, 89, 17176−17186 Read Online

ABSTRACT: The mechanism of the dirhodium-catalyzed combined C−H functionalization/Cope rearrangement (CH/Cope) reaction discovered by the Davies group has been investigated with density functional theory (DFT) calculations and quasi-classical molecular dynamics (MD) simulations. Computations from the Davies group previously showed that there is a post-transition state bifurcation leading to a direct CH reaction and also to the CH/Cope product. While this work was in preparation, the Tantillo group and the Ess group independently reported quantum mechanical and molecular dynamics studies on the dirhodium-tetracarboxylate-catalyzed diazoester CH/Cope and CH insertion reactions with 1,3-cyclohexadiene and 1,4-cyclohexadiene, respectively. The Tantillo group cited "dynamic mismatching" to explain the origins of the low yield of CH/Cope products in some experiments; the Ess group explained the origins of product selectivity from the perspective of TS vibrational modes and their synchronization that occurs at the entropic intermediates. We report quasi-classical trajectories for the reaction of the carbene with 1-methylcyclohexene that afford both the CH/Cope and C−H insertion products. After passing through the transition state that involves mostly hydrogen transfer, momentum drives the reaction trajectories toward the CH/Cope products.

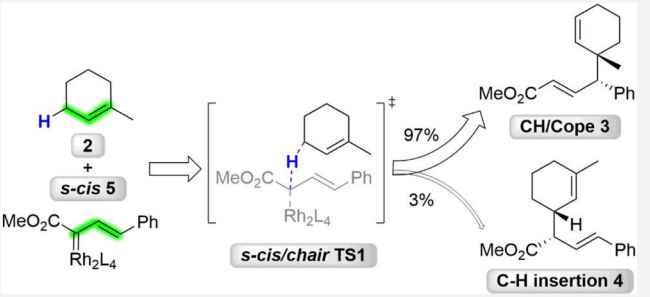

INTRODUCTION

Transition metal-catalyzed C−H bond functionalizations have become excellent strategies for the synthesis of complex organic molecules and the diversification of natural products.[1] A general method for C−H bond functionalization is the insertion of a metal carbenoid into a C−H bond.[2] The Davies group has pioneered the study of dirhodium tetracarboxylate catalysts for the insertion of a rhodium carbenoid into C−H bonds.[3] They also discovered the combined C−H functionalization/Cope rearrangement (CH/Cope) reaction, called CHCR by Davies et al.[4] Many effective synthetic methods for catalytic asymmetric transformations have been demonstrated by the Davies group.[5] In the late 1990s, the Davies group focused on the chemistry of C−H functionalization of aryldiazoacetates.[3,6] They discovered the combined C−H activation/Cope rearrangement, which we call CH/Cope for additional clarity.[4] They subsequently used this reaction to complete the total synthesis of complex natural products, such as (−)-colombiasin A,[1] (+)-elisapterosin B,[1] and (+)-erogorgiaene.[1] The Davies group also conducted a combination of theoretical and experimental studies to demonstrate the mechanism of the combined C−H activation/Cope rearrangement reaction of styryldiazoacetate **1** with 1-methylcyclohexene **2** (Scheme 1a), and showed that the CH/Cope reaction to form **3** is a concerted and highly asynchronous process.[7] Experiments showed that **3** undergoes a quantitative Cope rearrangement to **4** at 110 °C (Scheme 1b);[8] consequently, a two-step C−H activation and Cope rearrangement for the formation of the CH/Cope product **3** was ruled out.

The Davies group showed that there is a potential energy surface bifurcation leading to the CH/Cope reaction and the competing direct C−H insertion reaction from a single transition state (Scheme 1c). Both of these processes go through the same transition state **TS1** (Scheme 1d),[7] leading to a mixture of **3** and **4**. In **TS1**, the allylic C−H bond of 1-methylcyclohexene **2** undergoes cleavage. This results in the formation of either the C−H insertion product **4**, where the carbon−carbon bond between C_1−$C_{1'}$ is created or the CH/Cope product **3**, where the carbon−carbon bond between C_3−$C_{3'}$ is formed. The chairlike transition state model **TS1** was proposed by Davies et al., and it predicts the stereoselectivity of the CH/Cope reaction successfully.[7] The interesting discovery by the Davies group prompted us to work together to use the combination of more reliable DFT calculations and quasi-classical molecular dynamics (MD) simulations to elucidate the time-resolved mechanisms of the CH/Cope

Received: July 5, 2024
Revised: October 23, 2024
Accepted: November 1, 2024
Published: November 19, 2024

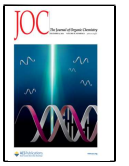

Scheme 1. Competing CH/Cope and Direct C−H Insertion

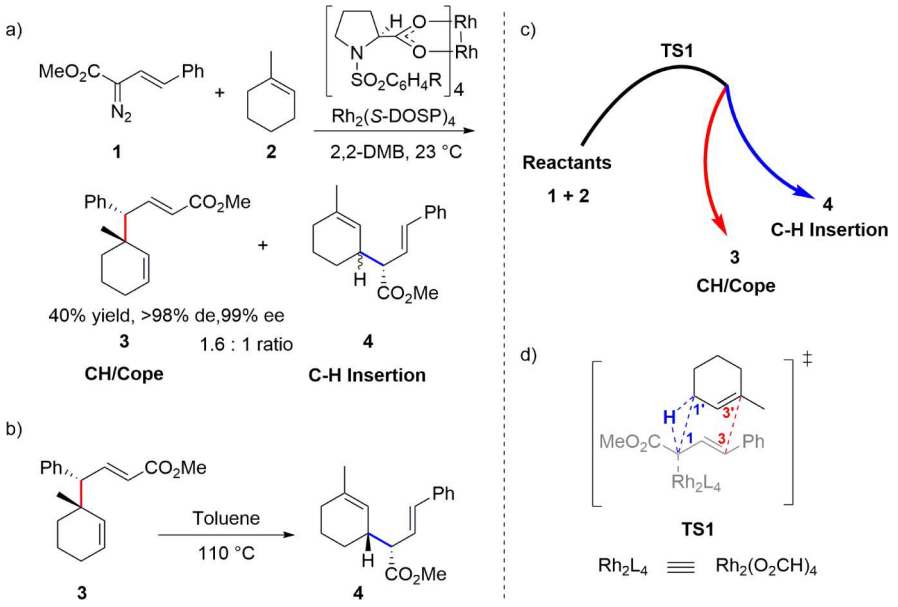

reaction and the direct C−H insertion on a femtosecond time-scale and to analyze the origin of product selectivity in this ambimodal reaction. Tantillo and coworkers carried out quasi-classical molecular dynamics studies on dirhodium-catalyzed C−H insertion reactions, leading to the formation of β-lactones.[9] Many additional DFT MD studies have provided time-resolved mechanistic insights to elaborate the dynamic factors that control selectivity in organometallic reactions.[10]

We have studied computationally the mechanism of the reaction of styryldiazoacetate **1** with 1-methylcyclohexene **2** catalyzed by Rh_2(*S*-DOSP)$_4$, which generates a 1.6:1 mixture of the CH/Cope product **3** and the direct C−H insertion product **4** (Scheme 1a).[8]

The traditional transition state theory successfully predicts the stereoselectivity of this reaction but fails to address the ambimodal selectivity of this reaction. Therefore, using quasi-classical molecular dynamics (MD) simulations, we studied the time-resolved mechanism of this reaction and explored the product selectivity.

While this manuscript was in preparation, the Tantillo group[11] and the Ess group[12] independently reported quantum mechanical and molecular dynamics studies of the dirhodium-tetracarboxylate-catalyzed reactions of diazoesters to give CH/Cope and CH insertion reactions with 1,3-cyclohexadiene and 1,4-cyclohexadiene, respectively. Their studies revealed the presence of entropic intermediates with zwitterionic character in MD simulation trajectories, underscoring their significant role in controlling product selectivity. The Tantillo group proposed the term "dynamic mismatching"[11] to contrast with Carpenter's "dynamic matching",[13] and to explain the observed dynamic behavior, in which a large amount of CH/Cope products were generated and several small amounts of additional side products were generated (consistent with experimental results). The Ess group explained the origins of product selectivity from the perspective of TS vibrational modes and their synchronization that occurs at the entropic intermediates.[12] In our study, we complement this perspective by elucidating the dynamic factors that control the formation of CH/Cope and C−H insertion products, emphasizing geometries of ambimodal transition states and bond orders of partial bonds in transition states. The results of the CH/Cope and CH insertion reactions of the phenyl carbenoid ester involving 1-methylcyclohexene are compared to the results of Tantillo and Ess later in this manuscript.

COMPUTATIONAL METHODS

DFT calculations were carried out with Gaussian 16.[14] Geometry optimizations and energy calculations were performed with B3LYP-D3.[15] Inclusion of dispersion with D3 is expected to ensure accuracy. The LANL2DZ basis set[16] with ECP was used for the Rh atom, and the 6-31G*[17] basis set was used for other atoms. Frequency analysis was conducted at the same level of theory to verify the stationary points to be real minima or saddle points and to obtain thermodynamic energy corrections. The single-point energies with solvation were calculated at the B3LYP-D3/6-311+G**[18]−SDD[19] level using the IEFPCM[20] solvation model (solvent = 2,2-DMB, ε = 1.86). The Gibbs free energy profiles with solvation correction at this level are very similar to those in the gas phase at the geometry optimization level (Table S1). The solvent effect is not included with MD calculation, because the C−H functionalization reaction is usually carried out in hydrocarbon solvents with very low dielectric constants (such as hexane, pentane, or 2,2-dimethylbutane).[7] Computed structures are illustrated using CYLview.[21]

The minimum-energy reaction path (MERP) connecting the transition structure to the C−H insertion product from the reacting complex was computed using the nudged elastic band method with the climbing image (NEB-CI) approach.[22] NEB-CI calculations were performed at the level of B3LYP-D3/6-31G*−LANL2DZ with ORCA 5.0.1.[22]

Quasi-classical MD simulations were performed at the level of B3LYP-D3/6-31G*−LANL2DZ by interfacing Singleton's ProgDyn code[23] with Gaussian 16. The initial configurations were generated by normal-mode sampling. Along the forward and reverse directions, molecular configurations and velocities were propagated using the velocity Verlet algorithm with a time step of 1 fs until the expected starting reactant or product was formed. Thresholds for bond formations and trajectory are

https://doi.org/10.1021/acs.joc.4c01682
J. Org. Chem. 2024, 89, 17176−17186

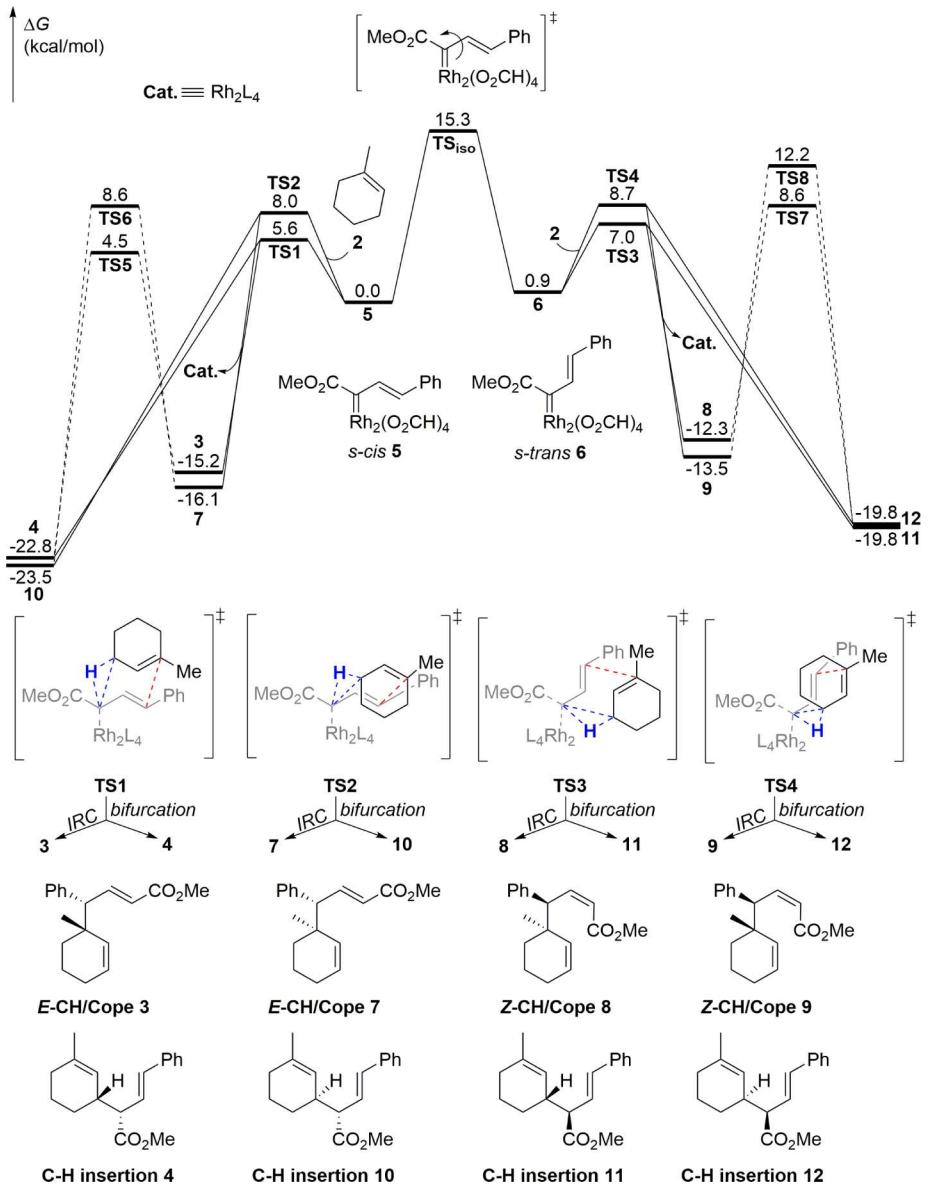

Figure 1. Gibbs free energy profiles for the reaction between rhodium vinylcarbenoid and 1-methylcyclohexene. Gibbs free energies were obtained at the B3LYP-D3/6-31G*−LANL2DZ level.

shown in Table S2. The root-mean-square deviation (RMSD) values between two structures were calculated by VMD.[24]

RESULTS AND DISCUSSION

Mechanism of Dirhodium-Catalyzed CH/Cope Reaction and Direct C−H Insertion. Studies by Davies et al. suggest that the CH/Cope reaction proceeds via a concerted mechanism with the allylic C−H bond cleaving and C−C bond forming asynchronously.[7,25] Styryldiazoacetate **1** exists in both the *s-cis* and *s-trans* conformations. The *s-cis* conformation is slightly favored by 0.6 kcal/mol (Figure S1). The dirhodium tetraprolinate catalyst Rh_2(*S*-DOSP)$_4$ is modeled here as $Rh_2(O_2CH)_4$ for computational efficiency since we have not explored stereoselectivity. The free energy profile for the formation of the rhodium carbenoid is shown in Figure S2. Styryldiazoacetate **1** reacts with $Rh_2(O_2CH)_4$ to form the rhodium carbenoid **5** along with the expulsion of N_2. This process requires a barrier of 9.9 kcal/mol and is thermodynamically favorable by 23.7 kcal/mol.

Figure 1 shows the free energy surface for the reaction of *cis*- and *trans*-carbenoid **5** and **6**, reacting with 1-methylcyclohexene. The rhodium vinylcarbenoid has two configurations, *s-cis* **5** and *s-trans* **6**, and **6** is 0.9 kcal/mol higher than **5**. The conversion between **5** and **6** requires a barrier of 15.3 kcal/mol, resulting in a non-Curtin−Hammett situation. Products from both **5** and **6** are expected since both of these are expected to be formed from the reaction of the diazoalkane with the dirhodium catalyst.

The barriers for the CH/Cope reaction via *s-cis/chair* **TS1** and *s-cis/boat* **TS2** are 5.6 and 8.0 kcal/mol, respectively, with respect to *s-cis* **5**. The barriers for the CH/Cope reaction via *s-trans/chair* **TS3** and *s-trans/boat* **TS4** are 6.1 and 7.8 kcal/mol, respectively, with respect to *s-trans* **6**. While the energetics imply that only **TS1** and **TS3** would be most likely to compete energetically, we explored all four TSs.

The Davies group's studies showed that the reactions of rhodium carbenoid **5** or **6** with 1-methylcyclohexene **2** involve bifurcating energy surfaces.[7] The *s-cis* **5** reacts with 1-

https://doi.org/10.1021/acs.joc.4c01682
J. Org. Chem. 2024, 89, 17176−17186

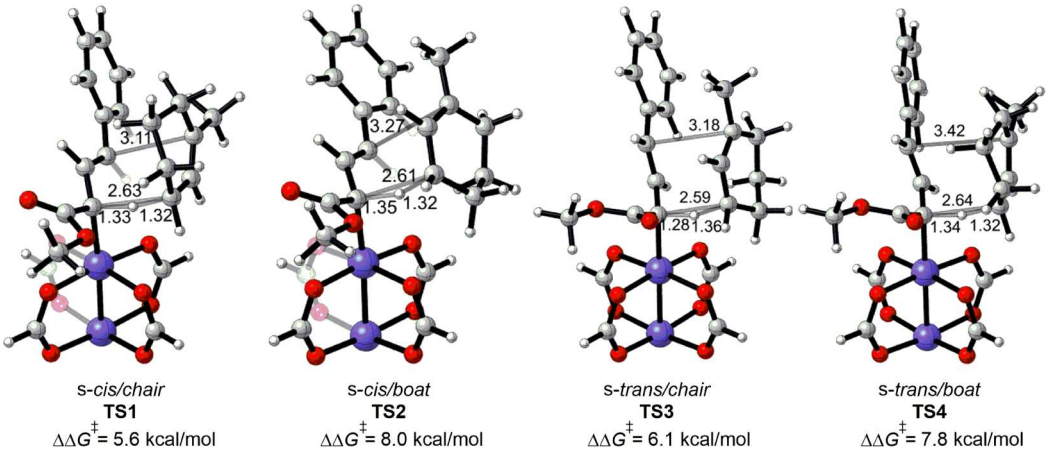

Figure 2. Optimized structures of four CH/Cope TSs. The selected bond distances are given in Å. Relative Gibbs free energies were obtained at the B3LYP-D3/6-31G*−LANL2DZ level.

methylcyclohexene **2** via *s-cis/chair* ambimodal **TS1** to form the *E*-CH/Cope product **3** and C−H insertion product **4**. The *E*-CH/Cope product **3** can undergo a facile Cope rearrangement transition state **TS5** ($\Delta\Delta G^{\ddagger}$ = 19.7 kcal/mol) to form the C−H insertion product **4**.

The *s-cis/chair* **TS1** is more stable than the *s-cis/boat* **TS2** by 2.4 kcal/mol. The *s-cis/boat* **TS2** leads to the *E*-CH/Cope product **7** and C−H insertion product **10**. Both have one inverted stereocenter compared to those of **3** and **4**. The *E*-CH/Cope product **7** can undergo a facile Cope rearrangement transition state **TS6** ($\Delta\Delta G^{\ddagger}$ = 24.7 kcal/mol) to form **10**.

Similarly, *s-trans* **6** reacts with 1-methylcyclohexene **2** via *s-trans/chair* **TS3** or *s-trans/boat* **TS4** to form the *Z*-CH/Cope products **8** or **9** and C−H insertion products **11** or **12**, respectively. The *Z*-CH/Cope products, **8** and **9**, can undergo facile Cope rearrangements via **TS7** ($\Delta\Delta G^{\ddagger}$ = 20.9 kcal/mol) and **TS8** ($\Delta\Delta G^{\ddagger}$ = 25.7 kcal/mol) to form the C−H insertion products, **11** and **12**, respectively. Note that C−H insertion products **4** and **12**, as well as C−H insertion products **10** and **11**, have different conformations of the carbonyl group. Figure 2 shows the optimized structures of the four ambimodal CH/Cope TSs, *s-cis/chair* **TS1**, *s-cis/boat* **TS2**, *s-trans/chair* **TS3**, and *s-trans/boat* **TS4**, that lead to four diastereomeric CH/Cope products (**3**, **7**, **8**, and **9**) and four diastereomeric C−H insertion products (**4**, **10**, **11**, and **12**).

The *s-cis* rhodium carbenoid **5** leads to the *E*-CH/Cope products, and the *s-trans* rhodium carbenoid **6** leads to the *Z*-CH/Cope products. In addition, the *chair* or *boat* conformation of CH/Cope TS determines the absolute configuration of the stereocenter substituted by the phenyl group. The ester substituent of the rhodium carbenoids *s-cis* **5** and *s-trans* **6** can rotate easily and result in two different conformations in CH/Cope TSs. In both **TS1** and **TS2**, the carbonyl group of the ester rotates away from the coming substrate 1-methylcyclohexene **2**, while in both **TS3** and **TS4**, the carbonyl group of the ester rotates toward the incoming substrate. The other four TSs, *s-cis/chair* **TS11** ($\Delta\Delta G^{\ddagger}$ = 6.0 kcal/mol) and *s-cis/boat* **TS12** ($\Delta\Delta G^{\ddagger}$ = 8.2 kcal/mol) with the carbonyl group toward the substrate, *s-trans/chair* **TS13** ($\Delta\Delta G^{\ddagger}$ = 6.8 kcal/mol) and *s-trans/boat* **TS14** ($\Delta\Delta G^{\ddagger}$ = 7.8 kcal/mol) with the carbonyl group away from the substrate, are shown in Figure S3. These TSs (**TS11**−**TS14**) are only slightly higher in energy than the conformers shown in Figure 2, but are expected to have very similar dynamic behavior. They were not studied further.

Computations from Davies et al. also gave four transition states analogous to **TS1**−**4**, using 1,3-cyclohexadiene and 1,4-cyclohexadiene as substrates in the same model system.[7] Their calculation results showed that the reaction through the *s-cis/chair* transition state ultimately leads to the CH/Cope products. Our calculations for 1-methylcyclohexene also show that the energy of *s-cis/chair* **TS1** is lowest ($\Delta\Delta G^{\ddagger}$ = 5.6 kcal/mol), and the computed intrinsic reaction coordinate (IRC) leads to the CH/Cope products with stereochemistry, in agreement with the experimental results.[8] Davies and coworkers found that the *s-trans* configuration has a kinetic preference for the generation of C−H bond insertion products from 1,4-cyclohexadiene as the substrate when using Rh_2(*S*-DOSP)$_4$ as a catalyst in the experiment.[7] To explain this, further in-depth analysis of the origins of product selectivity and the kinetic preferences of *s-cis* and *s-trans* configurations for products is performed here through molecular dynamics simulations.

Post-Transition State Bifurcations. We successfully located the CH/Cope product **3** and C−H insertion product **4**. The computed IRC led to **3**. In order to explore whether there exists another TS to form the C−H insertion product, we performed potential energy surface (PES) scans using the distances R1 and R2 as variables (see Figure 3). The resulting two-dimensional (2D) PES shown in Figure 3 clearly indicates the expected post-TS bifurcation with both the CH/Cope product **3** and the C−H insertion product **4** directly connected to **TS1**. In addition, there is a Cope rearrangement transition state (**TS5**) between the CH/Cope product **3** and the C−H insertion product **4**, as shown in Figure 3. The corresponding three-dimensional (3D) PES is shown in Figure S4.

Intrinsic reaction coordinate (IRC) calculations from the transition structure connect only a pathway from the reactant to the CH/Cope product. The C−H insertion product **4** was not connected to the transition structure in IRC calculations. To establish the nonintrinsic reaction coordinate (non-IRC) pathways to connect the C−H insertion product **4**, we employed the climbing image variant of the nudged elastic band (NEB-CI) approach in ORCA,[22] which located a minimum-energy reaction path (MERP) connecting the *s-cis* **5** and 1-methylcyclohexene **2** reactants to *s-cis/chair* **TS'** or **TS** and then to CH/Cope product **3** and C−H insertion product

https://doi.org/10.1021/acs.joc.4c01682
J. Org. Chem. 2024, 89, 17176−17186

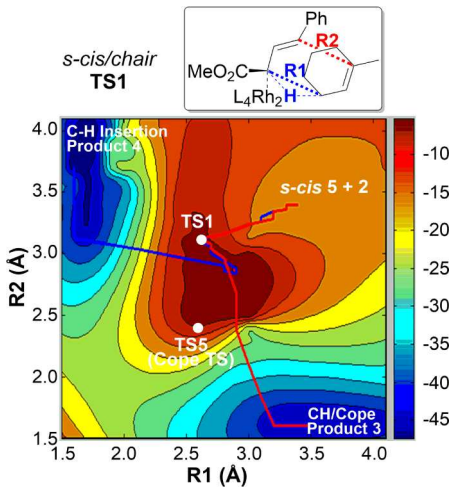

Figure 3. Potential energy surface through **TS1** as a function of R1 and R2. Electronic energies are relative to *s-cis* **5** and **2** and are shown in kcal/mol. The MERPs for **3** and **4** (see Figure 4) are shown as red and blue lines.

4, respectively. As shown in Figures 4 and 3, the reaction path indicated by the blue line goes through **TS1** and then forms a structure (**A**) resembling the subsequent Cope rearrangement transition state (R1 = 2.58 Å and R2 = 2.41 Å). The C−H bond is formed, and R1 (2.92 Å) and R2 (2.73 Å) indicate significant partial bonding. At structure **B**, R1 (2.50 Å) becomes shorter in length than R2 (2.88 Å), and after a sharp drop in energy, the C−C bond forms. The reaction path indicated by the red line goes through *s-cis/chair* **TS'** to form structure **A'**, then directly drops to form the CH/Cope product **3**.

As discussed by Tantillo[11] and Ess,[12] both studies predict the presence of entropic intermediates with zwitterionic characteristics in MD simulation trajectories. Tantillo's group has additionally observed instances where these entropic intermediates can transform into actual intermediates, suggesting the potential existence of shallow minima on the potential energy surface by optimizing the endpoints of the MD trajectories. In Figure 4, after passing through the hydride transfer transition state, we identified shallow minima at points **A** and **A'** on the potential energy surface using NEB-CI. However, recognizing the intrinsic errors of the computational methods used, we caution that these minima may represent artifacts rather than true stationary points. To further elucidate these structures, we conducted Mulliken spin density and natural bond orbital (NBO) charge analyses, as shown in Figure 5. We found the **TS'**(**TS**) involving a +0.24 charge on the methylcyclohexenyl moiety, which grows to approximately +0.40 in the regions **A** and **A'**. The shallow minimum containing **A** and **A'** on the MERP has significant zwitterionic character, and whether they can be characterized as entropic intermediates will be further explored by lifetimes in MD simulations.

Molecular Dynamics of the CH/Cope and C−H Insertion Reactions. Quasi-classical trajectory simulations were performed for each of the four TSs, **TS1**−**TS4**. Figure 6 shows two typical trajectories from *s-cis/chair* **TS1**, the starting point for the trajectories that result mainly in the formation of two products, CH/Cope product **3** and C−H insertion product **4**. The number of MD trajectories and the ratio of the two competing products are given in Table 1. The quasi-

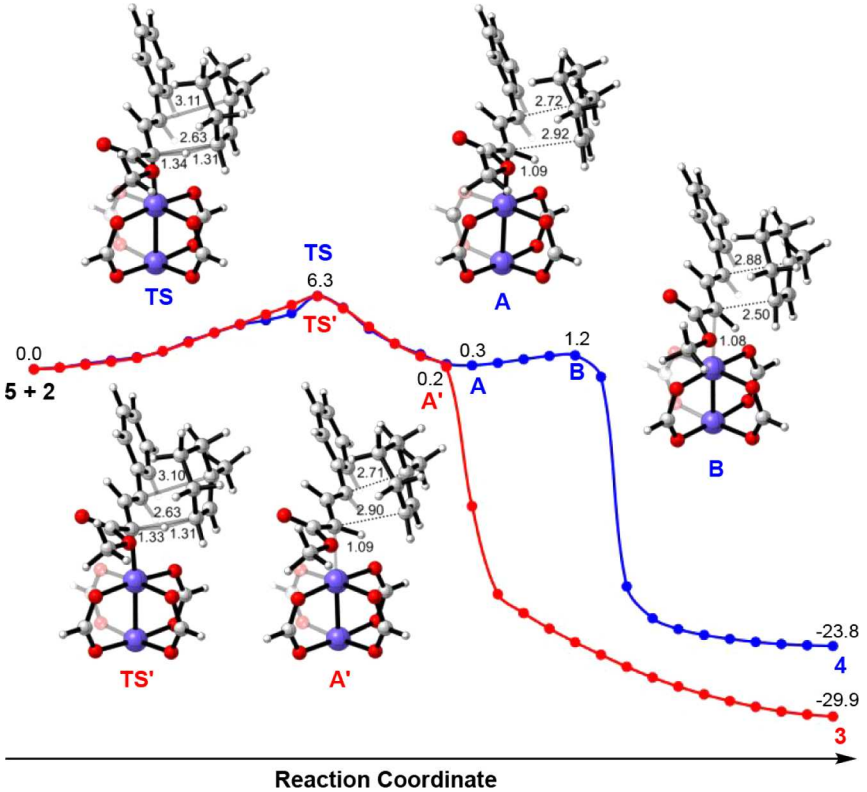

Figure 4. Minimum-energy reaction paths connecting *s-cis/chair* **TS'** to CH/Cope product **3** and *s-cis/chair* **TS** to C−H insertion product **4**. All electronic energies are relative to *s-cis* **5** and **2** and are shown in kcal/mol. The selected bond distances are given in Å.

https://doi.org/10.1021/acs.joc.4c01682
J. Org. Chem. 2024, 89, 17176−17186

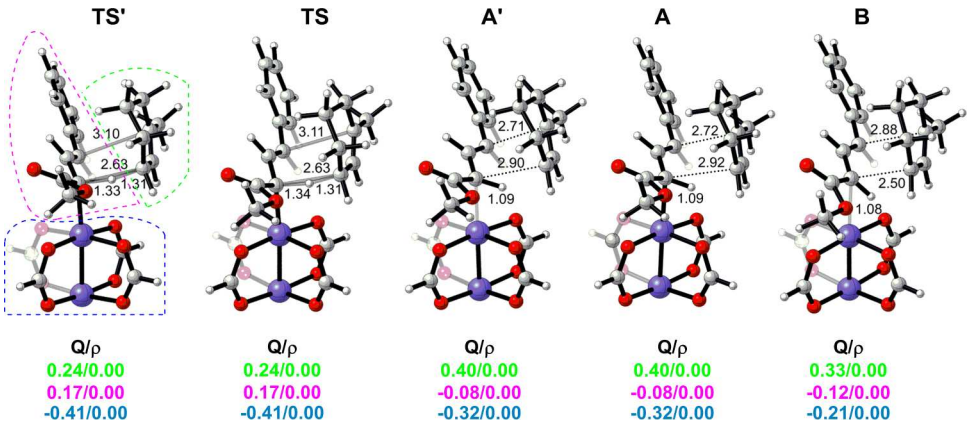

Figure 5. Populations of NBO charges (Q in e) and Mulliken spin densities (r) for *s-cis/chair* **TS'**, *s-cis/chair* **TS**, **A'**, **A**, and **B**. The NBO charges and Mulliken spin densities given below each structure are the total charges on the atoms enclosed in the region by the dashed lines of the same color.

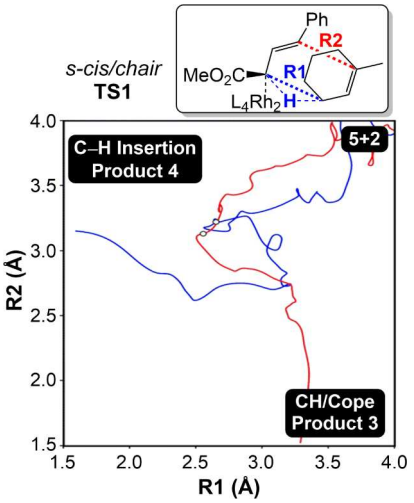

Figure 6. Two typical trajectories from the reaction dynamics simulation through **TS1**. White dot marks indicate sampled TS points used to initiate trajectories.

Table 1. Dynamics Results with Trajectories Initiated from TSs

	Total Trajectories	Reactive Trajectories	CH/Cope Product	C–H Insertion Product
TS1	432	286	277 (97%)	9 (3%)
TS2	470	310	266 (86%)	44 (14%)
TS3	543	338	13 (4%)	325 (96%)
TS4	475	282	189 (67%)	93 (33%)

classical trajectories starting from the four initial transition structures with different configurations are also shown in Figure 7. In a total of 432 trajectories propagated from the lowest-energy **TS**, *s-cis/chair* **TS1**, there are 286 productive trajectories leading to the products, and 137 recrossing (37 trajectories from the reactant to reactant, 98 trajectories from the CH/Cope product to the CH/Cope product, and 2 trajectories from the C–H insertion product to the C–H insertion product) trajectories. Out of the 286 reactive trajectories through **TS1**, 277 trajectories (97%) lead to *E*-CH/Cope product **3**, while only 9 trajectories (3%) go to C–H insertion product **4**. MD trajectories through *s-cis/boat* **TS2**, which is 2.4 kcal/mol higher in energy barrier than **TS1**, afford a ratio of 86:14 for *E*-CH/Cope product **7** and the direct C–H insertion product **10**.

The MD trajectories through *s-trans/chair* **TS3**, which is only 0.5 kcal/mol higher than **TS1**, show a 96:4 preference for the formation of the direct C–H insertion product **11** over the *Z*-CH/Cope product **8**. Although the IRC calculations show that **TS3** connects to *Z*-CH/Cope product **8**, the MD trajectory simulations demonstrate that the direct C–H insertion path is the dominant reaction path. This is unique since the other three TSs always favor the CH/Cope product. For MD trajectories through *s-trans/boat* **TS4**, a ratio of 67:33 for *Z*-CH/Cope product **9** over the direct C–H insertion product **12** is obtained.

In all the trajectories of the above four TSs, 30–40% of the trajectories are recrossing trajectories.[13] Many of these trajectories go through a weakly bound intermediate flat zone after passing through the TS zone, especially for the trajectories propagated from *s-trans/boat* **TS4**. The MD trajectories via **TS1**, **TS2**, and **TS4** show that the bifurcation of the hydrogen transfer transition states leads primarily to the CH/Cope products, as proposed by the Davies group,[7] while the higher energy **TS3** favors the direct CH insertion. In recent studies on the same system but with cyclohexadienes, the Tantillo[11] and Ess groups[12] have shown similar results in MD trajectories.

We also analyzed the time gaps between forming C–H and C–C bonds. The distribution of the time gaps between the formation of C–H and C–C bonds in the trajectories generating the CH/Cope product and C–H insertion product propagated from **TS1** (a), **TS2** (b), **TS3** (c), and **TS4** (d) is shown in Figure 8. The reaction is dynamically stepwise (time gap of formation of two bonds, τ > 60 fs[26]): the hydrogen transfer is quickly completed, and then after 64–1408 fs, the C–C bond forms to give the product. The rather long lifetime (>1000 fs) of the dynamic entropic intermediates[27] was found in some trajectories from **TS4**. In addition, in the 282 reactive trajectories propagated from *s-trans/boat* **TS4**, we find 8 trajectories connecting *s-cis* **5** with 1-methylcyclohexene **2** to the weakly bound intermediates. The TSs lead to three different species: CH/Cope product, C–H insertion product, and a weakly bound intermediate. The weakly bound intermediates are observed from the trajectories in a region with no potential energy minimum, suggestive of the existence of an entropic intermediate.[27] Tantillo[11] and Ess[12] both

https://doi.org/10.1021/acs.joc.4c01682
J. Org. Chem. 2024, 89, 17176–17186

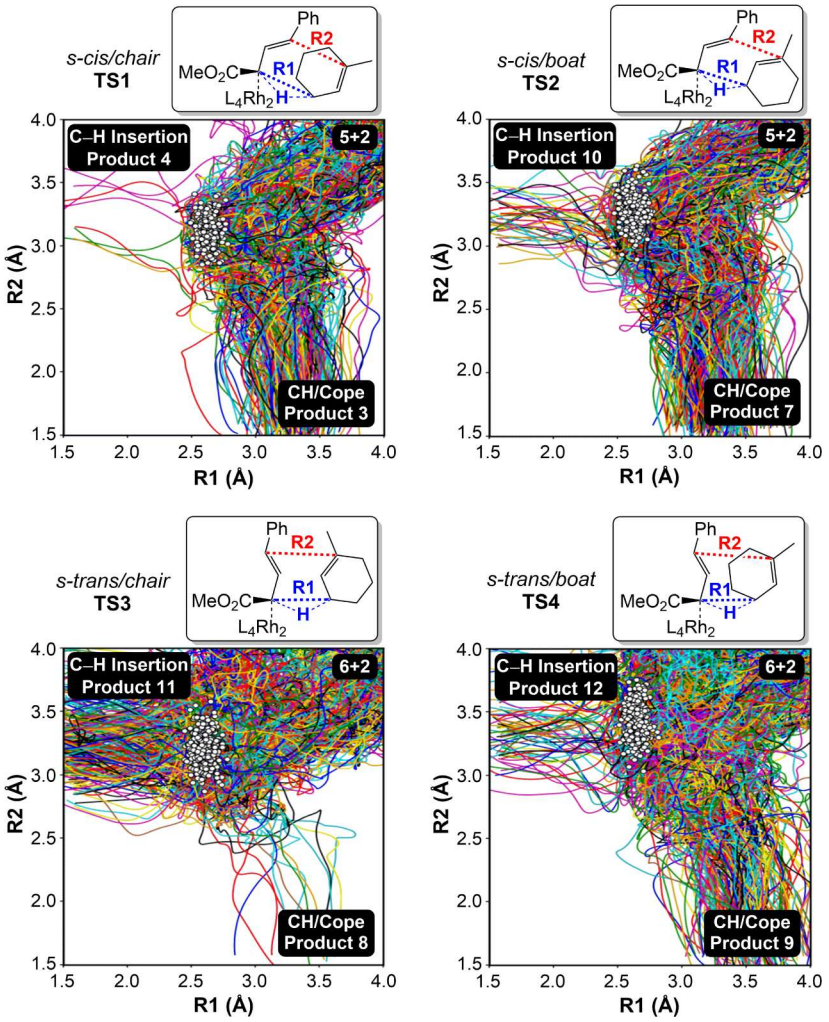

Figure 7. Plots of quasi-classical trajectories propagated from **TS1**, **TS2**, **TS3**, and **TS4**. The white dots are the locations of the normal-mode sampled points used to initiate trajectories.

characterized the presence of the entropic intermediate with a long lifetime in the CH/Cope reaction with 1,3-cyclohexadiene and 1,4-cyclohexadiene.

It is important to emphasize that the simulations indicate a strong preference for generating CH/Cope products over C−H insertion products in **TS1**, with this preference reversed in **TS3**. From a structural perspective, as shown in Figure 2, **TS1** exhibits a forming R1 bond length of 2.63 Å and R2 of 3.11 Å, and favors the formation of CH/Cope products. **TS3** displays an R1 bond length of 2.59 Å and R2 of 3.18 Å, shifting the ratio toward C−H insertion products. Based on the partial bond length model proposed by Houk and coworkers,[28] a shorter R2 and longer R1 in **TS1** align with the trend toward higher CH/Cope product formation, while in **TS3**, the changes in R2 and R1 lengths correlate with more C−H insertion product formation.

We also calculated the root-mean-square deviation (RMSD) between the transition states and the product structures. Houk and coworkers observed a good linear inverse correlation between structural similarities of the TS and each of the products − measured by the RMSD (between the ambimodal TS and the various products) − and the percentage of each of the products formed in MD simulations.[29] This was shown to be a useful metric to predict product ratios in ambimodal cycloadditions.[29] As shown in Table 2, the smaller RMSD value correctly indicates the major product for **TS1**−**TS3** but fails for **TS4**. The selectivity in **TS4** could be due to the formation of an entropic or actual intermediate,[27] sufficiently long-lived to undergo intramolecular vibrational energy redistribution (IVR), which can lead to a preference for CH/Cope product formation along the minimum energy path.

Momentum at the TS may also play a role in controlling product selectivity, as proposed by Carpenter − "dynamic matching."[13] After the hydrogen transfer transition state, the momentum favors the formation of CH/Cope products. As shown in Figures 3 and 6, after **TS1**, in both a trajectory leading to C−H insertion products (blue line) or CH/Cope products (red line), the reaction trajectories on the potential energy surface tend to move more toward the CH/Cope products as they move through the TS. We also analyzed two typical trajectories passing through *s-trans/chair* **TS3**. As shown in Figure 9, momentum is insufficient to drive a trajectory toward the product, but instead, the zwitterionic species spends time in a region best described as an entropic intermediate. That is what Tantillo describes as "dynamic mismatching."[11] The average time also increased correspondingly to 445 fs (see Figure 8c). The Tantillo group proposed the term "dynamic mismatching", which involves active momentum that drives trajectories away from forming the expected major product. This effect prolongs the lifetime of the

https://doi.org/10.1021/acs.joc.4c01682
J. Org. Chem. 2024, 89, 17176−17186

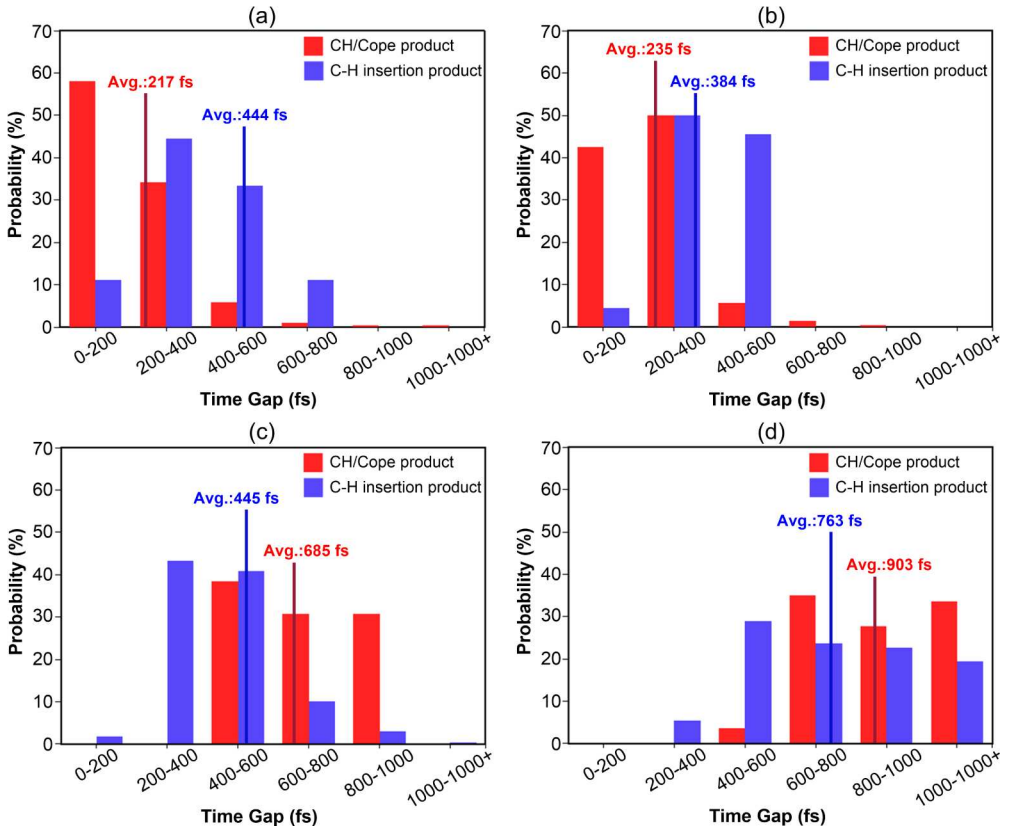

Figure 8. Distribution of the time gap between the formation of the C−H and C−C bonds in the trajectories generating the CH/Cope product and the C−H insertion product propagated from **TS1** (a), **TS2** (b), **TS3** (c), and **TS4** (d).

Table 2. RMSD Values between the Transition States and the Products

	RMSD			
	TS1	**TS2**	**TS3**	**TS4**
CH/Cope product	1.54 Å	1.68 Å	2.26 Å	2.55 Å
C−H insertion product	1.75 Å	1.93 Å	1.75 Å	2.21 Å

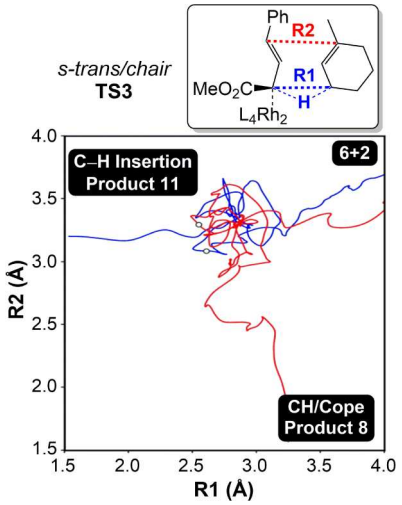

Figure 9. Two typical trajectories from reaction dynamics simulations through **TS3**. White dotted marks indicate sampled TS points used to initiate trajectories.

ion pair entropic intermediate, thereby contributing to the observed low yield of the CH/Cope product.[11] In Ess' work, a more detailed explanation of momentum factors is provided by exploring the vibrational synchronization between the key vibrational modes.[12] These three studies analyze the origins of product selectivity from distinct perspectives, each offering different insights into the origin of selectivity of the CH/Cope reaction.

In the case of the 1-methylcyclohexene substrate, the *s-cis* and *s-trans* configurations exhibit different kinetic preferences, which are consistent with the MD simulation trajectory results involving 1,3-cyclohexadiene[11] and 1,4-cyclohexadiene,[12] respectively. The dynamics trajectories confirm the conclusion of the Davies study, indicating that the *s-cis* configuration is conducive to the generation of CH/Cope products, and the *s-trans* configuration is more conducive to the generation of C−H insertion products. Differently, we analyzed the origins of product selectivity between CH/Cope products and C−H insertion products from the configuration similarity between the hydrogen atom transfer transition state and two different products. The smaller the RMSD value between the transition structure and a certain product, the more MD trajectories there are to generate that product.

The computational studies reveal that even though the *s-cis/chair* TS is the most favorable, the other three TSs are still relatively accessible. This explains why the high diastereoselectivity observed in CH/Cope reactions can be switched depending on the functionality of the vinyl carbene and the allylic substrate. For example, the vast majority of the reactions have been conducted with *E*-vinyldiazoacetates and are highly diastereoselective, forming essentially a single diastereomer, as illustrated in Figure 10a.[4b] Even though both the *s-trans* and *s-cis* configurations of the carbene are accessible, the reactions

https://doi.org/10.1021/acs.joc.4c01682
J. Org. Chem. 2024, 89, 17176−17186

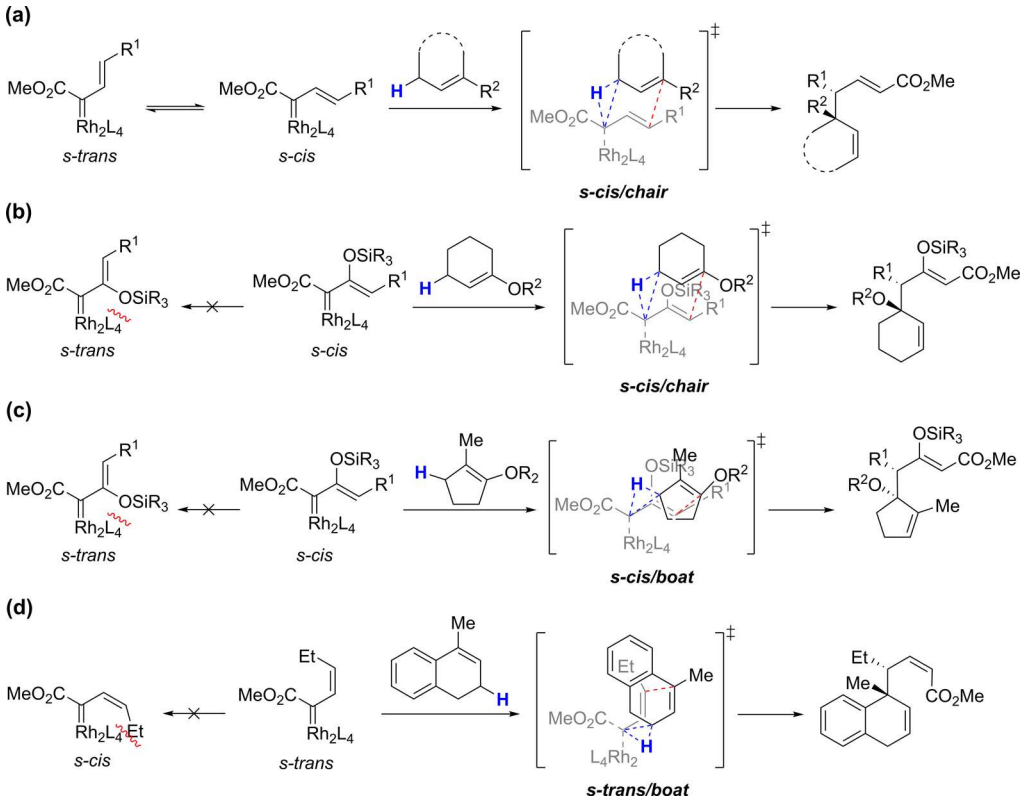

Figure 10. (a) Stereochemical outcome with *E*-vinyldiazoacetates (most common system); (b) stereochemical outcome with internally substituted vinyldiazoacetates with cyclohexene derivatives; (c) stereochemical outcome with internally substituted vinyldiazoacetates with cyclopentene derivatives; (d) stereochemical outcome with *Z*-vinyldiazoacetates.

proceed through the *s-cis/chair* TS, consistent with the preferred transition state determined in these computational studies. When the vinylcarbene has an internal siloxy substituent, the carbene must react through the *s-cis* configuration (Figure 10b,c) because the siloxy group in the *s-trans* configuration will point toward the catalyst wall.[25b] However, the reaction can lead to opposite stereochemical results depending on the structure of the allyl functionality. When the substrate is a cyclohexene derivative, the reaction proceeds through the *s-cis/chair* TS to avoid interference between the remainder of the cyclohexene structure and the wall of the catalyst (Figure 10b). By contrast, when the substrate is an internally methyl-substituted cyclopentene derivative, the reaction proceeds through the *s-cis/boat* TS to avoid interference of the methyl substituent with the catalyst's wall (Figure 10c). Finally, a CH/Cope reaction proceeding through the *s-trans/boat* TS is feasible when *Z*-vinyldiazoacetate is used (Figure 10d).[7] In this case the *s-cis* configuration of the vinylcarbene is not viable because the ethyl group will point toward the catalysts and is sterically inaccessible.

MD simulations on model systems provide valuable insights into the origins of selectivity, but these simulations inherently simplify the complexity of real catalysts like $Rh_2(DOSP)_4$. Despite these simplifications, our computational studies on the truncated model give a detailed picture of the mechanism of the CH/Cope reactions. These findings are complemented by experimental validations, underscoring the utility of our approach in guiding experimental design and interpretation.

CONCLUSIONS

We find that the CH/Cope reaction proceeds via a concerted mechanism with the allylic C−H bond cleaving and C−C bond forming asynchronously, as proposed in earlier work by Davies and coworkers. There is a post-transition state bifurcation during a dirhodium-catalyzed combined CH/Cope reaction, from which direct C−H insertion can also occur.

We performed MD simulations on four TSs and found that the two lowest energy TSs differ slightly and give opposite preferences for CH/Cope vs CH insertion. The *s-cis/chair* **TS1** gives 97% CH/Cope product and only 3% of the C−H insertion product. The *s-trans/chair* **TS3**, which is only 0.5 kcal/mol higher than the barrier through **TS1**, gives 96% of the C−H insertion product and only 4% of the CH/Cope product. Although we have not explored all the variations in substituted diazoacetates and cycloalkenes that have been studied, there is experimental evidence through product stereochemistries that each of the low-energy transition states is involved in reactions of appropriately substituted substrates. We analyzed the origins of product selectivity between CH/Cope products and C−H insertion products in these reactions of the dirhodium carbenoid with 1-methylcyclohexene. The ambimodal selectivity is controlled by the structural similarity of the products to the ambimodal TS (measured by the RMSD) and the bond strengths of partial bonds in the TSs. After passing through the transition state that involves mostly hydrogen transfer, momentum drives the reaction trajectories toward the CH/Cope products. We make conclusions about how the stereochemistries and product ratios are controlled by the ambivalent transition states of these reactions.

https://doi.org/10.1021/acs.joc.4c01682
J. Org. Chem. 2024, 89, 17176−17186

■ ASSOCIATED CONTENT

Data Availability Statement

The data underlying this study are available in the published article and its Supporting Information.

Supporting Information

The Supporting Information is available free of charge at https://pubs.acs.org/doi/10.1021/acs.joc.4c01682.

Calculated free energies of **TS1**, **TS2**, **TS3**, **TS4**, and $\mathbf{TS_{iso}}$; thresholds for bond formations and trajectory terminations; configurational change of styryldiazoacetate **1**; Gibbs free energy profiles for the formation of the rhodium carbenoid; optimized structures of **TS11**−**TS14**; three-dimensional (3D) potential energy surface; table of energies; cartesian coordinates of all structures and energies investigated in this work; NEB-CI results with energies and coordinates; initial TS sampling structures, velocities, and representative trajectories (PDF)

■ AUTHOR INFORMATION

Corresponding Authors

Huw M. L. Davies − *Department of Chemistry, Emory University, Atlanta, Georgia 30322, United States;* orcid.org/0000-0001-6254-9398; Email: hmdavie@emory.edu

Yun-Fang Yang − *College of Chemical Engineering, State Key Laboratory Breeding Base of Green-Chemical Synthesis Technology, Zhejiang University of Technology, Hangzhou, Zhejiang 310014, China;* orcid.org/0000-0002-6287-1640; Email: yangyf@zjut.edu.cn

K. N. Houk − *Department of Chemistry and Biochemistry, University of California, Los Angeles, California 90095, United States*; Email: houk@chem.ucla.edu

Authors

Yaling Zhang − *College of Chemical Engineering, State Key Laboratory Breeding Base of Green-Chemical Synthesis Technology, Zhejiang University of Technology, Hangzhou, Zhejiang 310014, China; Department of Chemistry and Biochemistry, University of California, Los Angeles, California 90095, United States*

Chaoqin Cao − *College of Chemical Engineering, State Key Laboratory Breeding Base of Green-Chemical Synthesis Technology, Zhejiang University of Technology, Hangzhou, Zhejiang 310014, China*

Yuanbin She − *College of Chemical Engineering, State Key Laboratory Breeding Base of Green-Chemical Synthesis Technology, Zhejiang University of Technology, Hangzhou, Zhejiang 310014, China;* orcid.org/0000-0002-1007-1852

Complete contact information is available at: https://pubs.acs.org/10.1021/acs.joc.4c01682

Notes

The authors declare no competing financial interest.

■ ACKNOWLEDGMENTS

Financial support from the National Natural Science Foundation of China (22138011, 22371256, and 21978272), the Fundamental Research Funds for the Provincial Universities of Zhejiang (RF-C2022006), the Province-Ministry Co-Construct State Key Laboratory of Green Chemistry-Synthesis Technology at Zhejiang University of Technology, and the US National Science Foundation (CHE-2153972 to KNH) and US National Institutes of Health (GM099142 to HMLD) is gratefully acknowledged.

■ REFERENCES

(1) (a) Davies, H. M. L.; Doan, B. D. Total Synthesis of (±)-Tremulenolide A and (±)-Tremulenediol A via a Stereoselective Cyclopropanation/Cope Rearrangement Annulation Strategy. *J. Org. Chem.* **1998**, *63*, 657−660. (b) Davies, H. M. L.; Venkataramani, C.; Hansen, T.; Hopper, D. W. New Strategic Reactions for Organic Synthesis: Catalytic Asymmetric C−H Activation α to Nitrogen as a Surrogate for the Mannich Reaction. *J. Am. Chem. Soc.* **2003**, *125*, 6462−6468. (c) Davies, H. M. L.; Jin, Q. Highly Diastereoselective and Enantioselective C−H Functionalization of 1,2-Dihydronaphthalenes: A Combined C−H Activation/Cope Rearrangement Followed by a Retro-Cope Rearrangement. *J. Am. Chem. Soc.* **2004**, *126*, 10862−10863. (d) Davies, H. M. L.; Walji, A. M. Direct Synthesis of (+)-Erogorgiaene through a Kinetic Enantiodifferentiating Step. *Angew. Chem., Int. Ed.* **2005**, *44*, 1733−1735. (e) Davies, H. M. L.; Dai, X.; Long, M. S. Combined C−H Activation/Cope Rearrangement as a Strategic Reaction in Organic Synthesis: Total Synthesis of (−)-Colombiasin A and (−)-Elisapterosin B. *J. Am. Chem. Soc.* **2006**, *128*, 2485−2490. (f) Hummel, J. R.; Boerth, J. A.; Ellman, J. A. Transition-Metal-Catalyzed C−H Bond Addition to Carbonyls, Imines, and Related Polarized π Bonds. *Chem. Rev.* **2017**, *117*, 9163−9227. (g) Khade, R. L.; Zhang, Y. C−H Insertions by Iron Porphyrin Carbene: Basic Mechanism and Origin of Substrate Selectivity. *Chem.—Eur. J.* **2017**, *23*, 17654−17658. (h) Lapuh, M. I.; Mazeh, S.; Besset, T. Chiral Transient Directing Groups in Transition-Metal-Catalyzed Enantioselective C−H Bond Functionalization. *ACS Catal.* **2020**, *10*, 12898−12919.

(2) Doyle, M. P.; Forbes, D. C. Recent Advances in Asymmetric Catalytic Metal Carbene Transformations. *Chem. Rev.* **1998**, *98*, 911−936. (b) Davies, H. M. L.; Manning, J. R. Catalytic C−H Functionalization by Metal Carbenoid and Nitrenoid Insertion. *Nature* **2008**, *451*, 417−424. (c) Doyle, M. P.; Duffy, R.; Ratnikov, M.; Zhou, L. Catalytic Carbene Insertion into C−H Bonds. *Chem. Rev.* **2010**, *110*, 704−724.

(3) Davies, H. M. L.; Hansen, T.; Hopper, D. W.; Panaro, S.-A.-H.-R. Highly Regio-, Diastereo-, and Enantioselective C−H Insertions of Methyl Aryldiazoacetates into Cyclic N-Boc-Protected Amines. Asymmetric Synthesis of Novel C_2 -Symmetric Amines and threo -Methylphenidate. *J. Am. Chem. Soc.* **1999**, *121* (27), 6509−6510.

(4) (a) Davies, H. M. L.; Stafford, D. G.; Hansen, T. Catalytic Asymmetric Synthesis of Diarylacetates and 4,4-Diarylbutanoates. A Formal Asymmetric Synthesis of (+)-Sertraline. *Org. Lett.* **1999**, *1*, 233−236. (b) Davies, H. M. L.; Lian, Y. The Combined C−H Functionalization/Cope Rearrangement: Discovery and Applications in Organic Synthesis. *Acc. Chem. Res.* **2012**, *45* (45), 923−935.

(5) (a) Davies, H. M. L.; Beckwith, R. E. J. Catalytic Enantioselective C−H Activation by Means of Metal−Carbenoid-Induced C−H Insertion. *Chem. Rev.* **2003**, *103*, 2861−2904. (b) Davies, H. M. L.; Morton, D. Guiding Principles for Site Selective and Stereoselective Intermolecular C−H Functionalization by Donor/Acceptor Rhodium Carbenes. *Chem. Soc. Rev.* **2011**, *40*, 1857−1869.

(6) (a) Davies, H. M. L.; Hansen, T.; Churchill, M. R. Catalytic Asymmetric C−H Activation of Alkanes and Tetrahydrofuran. *J. Am. Chem. Soc.* **2000**, *122*, 3063−3070. (b) Davies, H. M. L.; Antoulinakis, E. G. Recent Progress in Asymmetric Intermolecular C−H Activation by Rhodium Carbenoid Intermediates. *J. Organomet. Chem.* **2001**, *617*−*618*, 47−55.

(7) Hansen, J. H.; Gregg, T. M.; Ovalles, S. R.; Lian, Y.; Autschbach, J.; Davies, H. M. L. On the Mechanism and Selectivity of the Combined C−H Activation/Cope Rearrangement. *J. Am. Chem. Soc.* **2011**, *133*, 5076−5085.

(8) Davies, H. M. L.; Jin, Q. Catalytic asymmetric reactions for organic synthesis: The combined C−H activation/Cope rearrangement. *Proc. Natl. Acad. Sci. U.S.A.* **2004**, *101*, 5472.
(9) Guo, W.; Hare, S. R.; Chen, S.-S.; Saunders, C. M.; Tantillo, D. J. C−H Insertion in Dirhodium Tetracarboxylate-Catalyzed Reactions despite Dynamical Tendencies toward Fragmentation: Implications for Reaction Efficiency and Catalyst Design. *J. Am. Chem. Soc.* **2022**, *144*, 17219−17231.
(10) (a) Essafi, S.; Tew, D. P.; Harvey, J. N. The Dynamics of the Reaction of FeO+ and H2: A Model for Inorganic Oxidation. *Angew. Chem., Int. Ed.* **2017**, *56*, 5790−5794. (b) Carlsen, R.; Wohlgemuth, N.; Carlson, L.; Ess, D. H. Dynamical Mechanism May Avoid High-Oxidation State Ir(V)−H Intermediate and Coordination Complex in Alkane and Arene C−H Activation by Cationic Ir(III) Phosphine. *J. Am. Chem. Soc.* **2018**, *140*, 11039−11045. (c) Feng, Q.; Wu, H.; Li, X.; Song, L.; Chung, L. W.; Wu, Y.-D.; Sun, J. Ru-Catalyzed Geminal Hydroboration of Silyl Alkynes via a New gem-Addition Mechanism. *J. Am. Chem. Soc.* **2020**, *142*, 13867−13877. (d) Yang, Y.; Zhang, X.; Zhong, L.-P.; Lan, J.; Li, X.; Li, C.-C.; Chung, L. W. Unusual KIE and dynamics effects in the Fe-catalyzed hetero-Diels-Alder reaction of unactivated aldehydes and dienes. *Nat. Commun.* **2020**, *11* (1), 1850. (e) Zhang, Y.; Cao, C.; She, Y.; Yang, Y.-F.; Houk, K. N. Molecular Dynamics of Iron Porphyrin-Catalyzed C−H Hydroxylation of Ethylbenzene. *J. Am. Chem. Soc.* **2023**, *145*, 14446−14455. (f) Joy, J.; Ess, D. H. Direct Dynamics Trajectories Demonstrate Dynamic Matching and Nonstatistical Radical Pair Intermediates during Fe-Oxo-Mediated C−H Functionalization Reactions. *J. Am. Chem. Soc.* **2023**, *145*, 7628−7637. (g) Joy, J.; Schaefer, A. J.; Teynor, M. S.; Ess, D. H. Dynamical Origin of Rebound versus Dissociation Selectivity during Fe-Oxo-Mediated C−H Functionalization Reactions. *J. Am. Chem. Soc.* **2024**, *146*, 2452−2464. (h) Tantillo, D. J. Quantum Chemical Interrogation of Reactions Promoted by Dirhodium Tetracarboxylate Catalysts−Mechanism, Selectivity, and Nonstatistical Dynamic Effects. *Acc. Chem. Res.* **2024**, *57*, 1931−1940.
(11) Guo, W.; Tantillo, D. J. Running Wild through Dirhodium Tetracarboxylate-Catalyzed Combined CH(C)-Functionalization/Cope Rearrangement Landscapes: Does Post-Transition-State Dynamic Mismatching Influence Product Distributions? *J. Am. Chem. Soc.* **2024**, *146*, 7039−7051.
(12) Schaefer, A. J.; Ess, D. H. Vibrational synchronization and its reaction pathway influence from an entropic intermediate in a dirhodium catalyzed allylic C−H activation/Cope rearrangement reaction. *Phys. Chem. Chem. Phys.* **2024**, *26*, 11386−11394.
(13) (a) Carpenter, B. K. Dynamic Matching: The Cause of Inversion of Configuration in the [1,3] Sigmatropic Migration? *J. Am. Chem. Soc.* **1995**, *117*, 6336−6344. (b) Carpenter, B. K. Dynamic behavior of organic reactive intermediates. *Angew. Chem., Int. Ed.* **1998**, *37* (24), 3340−3350. (c) Reyes, M. B.; Carpenter, B. K. Mechanism of Thermal Deazetization of 2,3-Diazabicyclo[2.2.1]hept-2-ene and Its Reaction Dynamics in Supercritical Fluids. *J. Am. Chem. Soc.* **2000**, *122* (122), 10163−10176. (d) Carpenter, B. K. Nonstatistical Dynamics in Thermal Reactions of Polyatomic Molecules. *Annu. Rev. Phys. Chem.* **2005**, *56*, 57−89. (e) Wang, Z.; Hirschi, J. S.; Singleton, D. A. Recrossing and Dynamic Matching Effects on Selectivity in a Diels−Alder Reaction. *Angew. Chem., Int. Ed.* **2009**, *48*, 9156−9159. (f) Goldman, L. M.; Glowacki, D. R.; Carpenter, B. K. Nonstatistical Dynamics in Unlikely Places: 1,5] Hydrogen Migration in Chemically Activated Cyclopentadiene. *J. Am. Chem. Soc.* **2011**, *133*, 5312−5318.
(14) Frisch, M. J.; Trucks, G. W.; Schlegel, H. B.; Scuseria, G. E.; Robb, M. A.; Cheeseman, J. R.; Scalmani, G.; Barone, V.; Petersson, G. A.; Nakatsuji, H., et al.Vol. *16*; Gaussian, Inc.: Wallingford, CT, 2019.
(15) (a) Grimme, S.; Antony, J.; Ehrlich, S.; Krieg, H. A. A consistent and accurate ab initio parametrization of density functional dispersion correction (DFT-D) for the 94 elements H-Pu. *J. Chem. Phys.* **2010**, *132* (15), 154104. (b) Grimme, S.; Ehrlich, S.; Goerigk, L. Effect of the damping function in dispersion corrected density functional theory. *J. Comput. Chem.* **2011**, *32* (32), 1456−1465.
(16) (a) Hay, P. J.; Wadt, W. R. Ab initio effective core potentials for molecular calculations. Potentials for K to Au including the outermost core orbitals. *J. Chem. Phys.* **1985**, *82*, 299−310. (b) Ehlers, A. W.; Böhme, M.; Dapprich, S.; Gobbi, A.; Höllwarth, A.; Jonas, V.; Köhler, K. F.; Stegmann, R.; Veldkamp, A.; Frenking, G. A set of f-polarization functions for pseudo-potential basis sets of the transition metals Sc-Cu, Y-Ag and La-Au. *Chem. Phys. Lett.* **1993**, *208* (208), 111−114. (c) Roy, L. E.; Hay, P. J.; Martin, R. L. Revised Basis Sets for the LANL Effective Core Potentials. *J. Chem. Theory Comput.* **2008**, *4*, 1029−1031.
(17) (a) Ditchfield, R.; Hehre, W. J.; Pople, J. A. Self-Consistent Molecular-Orbital Methods. IX. An Extended Gaussian-Type Basis for Molecular-Orbital Studies of Organic Molecules. *J. Chem. Phys.* **1971**, *54*, 724−728. (b) Hehre, W. J.; Ditchfield, R.; Pople, J. A. Self—Consistent Molecular Orbital Methods. XII. Further Extensions of Gaussian—Type Basis Sets for Use in Molecular Orbital Studies of Organic Molecules. *J. Chem. Phys.* **1972**, *56*, 2257−2261.
(18) Krishnan, R.; Binkley, J. S.; Seeger, R.; Pople, J. A. Self-consistent molecular orbital methods. XX. A basis set for correlated wave functions. *J. Chem. Phys.* **1980**, *72*, 650−654.
(19) Dolg, M.; Wedig, U.; Stoll, H.; Preuss, H. Energy-adjusted ab initio pseudopotentials for the first row transition elements. *J. Chem. Phys.* **1987**, *86*, 866−872.
(20) Klamt, A.; Moya, C.; Palomar, J. A Comprehensive Comparison of the IEFPCM and SS(V)PE Continuum Solvation Methods with the COSMO Approach. *J. Chem. Theory Comput.* **2015**, *11*, 4220−4225.
(21) Legault, C. Y. CYLview, 1.0b; Université de Sherbrooke: Canada, 2009. http://www.cylview.org. (accessed 07 December 2021).
(22) (a) Neese, F. The ORCA program system. *Wiley Interdiscip. Rev.: comput. Mol. Sci.* **2012**, *2*, 73−78. (b) Legault, C. Y. Software update: The ORCA program system—Version 5.0. *Wiley Interdiscip. Rev.: Comput. Mol. Sci.* **2022**, *12* (5), No. e1606.
(23) Singleton, D. A.; Wang, Z. Isotope Effects and the Nature of Enantioselectivity in the Shi Epoxidation. The Importance of Asynchronicity. *J. Am. Chem. Soc.* **2005**, *127*, 6679−6685.
(24) Humphrey, W.; Dalke, A.; Schulten, K. Visual Molecular Dynamics. *J. Mol. Graph.* **1996**, *14* (1), 33−38.
(25) (a) Hansen, J.; Autschbach, J.; Davies, H. M. L. Computational Study on the Selectivity of Donor/Acceptor-Substituted Rhodium Carbenoids. *J. Org. Chem.* **2009**, *74*, 6555−6563. (b) Lian, Y.; Hardcastle, K. I.; Davies, H. M. L. Computationally Guided Stereocontrol of the Combined C−H Functionalization/Cope Rearrangement. *Angew. Chem., Int. Ed.* **2011**, *50*, 9370−9373.
(26) (a) Xu, L.; Doubleday, C. E.; Houk, K. N. Dynamics of Carbene Cycloadditions. *J. Am. Chem. Soc.* **2011**, *133*, 17848−17854. (b) Black, K.; Liu, P.; Xu, L.; Doubleday, C.; Houk, K. N. Dynamics, transition states, and timing of bond formation in Diels−Alder reactions. *Proc. Natl. Acad. Sci. U.S.A.* **2012**, *109* (109), 12860. (c) Hong, X.; Bercovici, D. A.; Yang, Z.; Al-Bataineh, N.; Srinivasan, R.; Dhakal, R. C.; Houk, K. N.; Brewer, M. Mechanism and Dynamics of Intramolecular C−H Insertion Reactions of 1-Aza-2-azoniaallene Salts. *J. Am. Chem. Soc.* **2015**, *137*, 9100−9107. (d) Patel, A.; Chen, Z.; Yang, Z.; Gutiérrez, O.; Liu, H.-W.; Houk, K. N.; Singleton, D. A. Dynamically Complex [6 + 4] and [4 + 2] Cycloadditions in the Biosynthesis of Spinosyn A. *J. Am. Chem. Soc.* **2016**, *138*, 3631−3634.
(27) Yang, Z.; Jamieson, C. S.; Xue, X.-S.; Garcia-Borràs, M.; Benton, T.; Dong, X.; Liu, F.; Houk, K. N. Mechanisms and Dynamics of Reactions Involving Entropic Intermediates. *Trends Chem.* **2019**, *1*, 22−34.
(28) Yang, Z.; Dong, X.; Yu, Y.; Yu, P.; Li, Y.; Jamieson, C.; Houk, K. N. Relationships between Product Ratios in Ambimodal Pericyclic Reactions and Bond Lengths in Transition Structures. *J. Am. Chem. Soc.* **2018**, *140*, 3061−3067.
(29) Martin-Somer, A.; Xue, X.-S.; Jamieson, C. S.; Zou, Y.; Houk, K. N. Computational Design of a Tetrapericyclic Cycloaddition and the Nature of Potential Energy Surfaces with Multiple Bifurcations. *J. Am. Chem. Soc.* **2023**, *145*, 4221−4230.

https://doi.org/10.1021/acs.joc.4c01682
J. Org. Chem. 2024, 89, 17176−17186